Magnetic filaments for anisotropic composite polymers

Laurence Ourry, Damien Le Roy, Samir Mekkaoui, Thierry Douillard,
Anne-Laure Deman, Vincent Salles

HAL Id: hal-02919884
https://hal.science/hal-02919884

Submitted on 26 Feb 2021

Magnetic filaments for anisotropic composite polymers

Laurence Ourry[1,2], Damien Le Roy[3], Samir Mekkaoui[2], Thierry Douillard[4],

Anne-Laure Deman[2], Vincent Salles[1,*]

[1] *Univ Lyon, Université Claude Bernard Lyon1, Laboratoire des Multimatériaux et Interfaces, UMR CNRS 5615, F-69622, Villeurbanne, France*

[2] *Univ Lyon, Université Claude Bernard Lyon1, Institut des Nanotechnologies de Lyon INL, UMR CNRS 5270, F-69622, Villeurbanne, France*

[3] *Univ Lyon, Université Claude Bernard Lyon1, Institut Lumière Matière ILM, UMR CNRS 5306, F-69622, Villeurbanne, France*

[4] *Univ Lyon, INSA Laboratoire Matériaux : Ingénierie et Science MATEIS, UMR CNRS 5510, F-69621, Villeurbanne, France*

* Corresponding author: vincent.salles@univ-lyon1.fr

Abstract

The use of contactless magnetic forces meets numerous needs in microelectromechanical systems (MEMS) or microfluidic devices. In this view, heterogeneous materials integrating magnetic nanostructures within a non-magnetic matrix such as polymer can produce local variations of magnetic field, at the sub-micrometer scale. Here we report on the synthesis of magnetic composites using electrospun nanofilaments and a polydimethylsiloxane (PDMS) matrix. Varying the precursor nature and heat treatment conditions, we obtained single phase filaments of Fe, FeNi, and MFe_2O_4 (M=Co, Fe, Ni). Thanks to a fine investigation of their structure and morphology, it was possible to measure from magnetically-soft ($\mu_0 H_C \leq 5$ mT) to relatively hard ($\mu_0 H_C$ up to 93 mT, M_R/M_S up to 0.5) behaviors. The common one-dimensional shape of these filaments leads to an anisotropic magnetic response. This can be exploited to achieve self-organization of the filaments in arrays within the non-magnetic matrix. We show the first step towards the development of magnetically anisotropic membranes of PDMS with 0.23wt% Fe filaments. These composite materials are promising for implementing magnetic functions in microsystems while circumventing complex micro-fabrication steps.

Keywords

1. Introduction

Magnetic composite polymers are part of new multifunctional materials that aroused considerable interest over the past two decades. The nature, size, concentration of the magnetic particles added in the polymer matrix modify the magnetic behaviors of the composite[1]. Magnetic multifunctional materials address numerous applications such as microelectromechanical systems (MEMS) for sensors and actuators [2–5] controlled drug delivery based on thermoresponsive materials or magnetic guidance [1], bioinspired microstructures [6,7], microfluidics functions such as micro-object trapping [8][9] or fluidics components [10][11].

Fine control of the magnetic properties is required to optimize their implementation. In particular, the development of composite materials with anisotropic magnetic properties opens up many perspectives. This magnetic anisotropy can be achieved through the creation of chains of magnetic particles or the use of magnetic nano- or micro-filaments. This first approach is versatile and easy to implement, through the application of a magnetic pattern during the composite fabrication, and permits to enhance the magnetic response in the direction of the chain[12–14]. S. Marchi et al. reported that the deflection of a composite polymeric membrane is increased when particles are aligned in the matrix and the magnetic field is applied along the chains, compared to disordered composite[15]. In the field of microfluidics, the increased magnetic susceptibility along the chains of particles, amplify generated magnetophoretic forces[16]. Besides, magnetic composite at relatively low concentration (up to 10 wt%), can form arrays of isolated and well-defined chains of magnetic particles homogeneously distributed within the polymer matrix. These structures were found to act as efficient magnetic flux micro-concentrators and were

used as micro-traps in microdevices [17], notably in the scope of single cell or single bead analysis systems [18][19]. Indeed, magnetic micro-traps permitted to capture thousands of isolated beads [10].

However, if the results are promising, the chains of particles are relatively porous, and so the magnetic flux guides are discontinuous [20]. In this regard, continuous magnetic structures with high aspect ratio, such as nanofibers, would be highly beneficial. The synthesis of magnetic nanofilaments with strong saturation magnetization and good dispersion in polymer matrixremains a challenge.

Magnetic composite polymers based on magnetic fillers with a cylindrical shape are reported in the literature,[4,21,22] , with fillers obtained using a porous and sacrificial template. This fabrication process presents a low production rate and is suitable for only a few materials. Since the beginning of the 21st century, numerous kinds of filaments have been produced using a unique and versatile process called "electrospinning" (ES). Briefly, a polymer solution is stretched under an electric field to produce solid filaments with a final diameter in the range of micrometer or nanometrer scale, with an adjustable production rate by sizing correctly the setup. More than polymer filaments, inorganic wires can be produced if metallic salts or specific precursors are introduced in the raw polymer solution.

Particularly, the state of the art on ES shows that a lot of oxide filaments have been produced and studied in the last two decades. Some of those articles are about electrospun magnetic (nano)filaments, made of cobalt [23], nickel [24] or iron oxides[25][26], or even of mixed Co/Fe [27] and Ni/Fe oxides[28]. Moreover, one can notice a previous work of our group dealing with the synthesis of electrospun iron carbide filaments used as fillers in a Polyurethane matrix[29]. To our knowledge, only

one article is related to the fabrication of pure iron electrospun filaments[30], but the authors did not study the magnetic properties of such nanomaterials.

The present study is part of the development of new multifunctional material, Fe magnetic nanofibers/PDMS (polydimethylsiloxane). PDMS matrix presents numerous advantages. This elastomer, widely used in microfluidics, is biocompatible, non-toxic, and easily micropatterned by soft-lithography. In addition, PDMS-based composites permit to solve issues linked to heterogeneous integration of magnetic materials with polymers.

We performed a complete study of structural and magnetic properties of electrospun fibers, with different chemical compositions and/or different metal oxidation degrees in view to select a PDMS filler combining a high magnetization at saturation and a good dispersion ability in the PDMS matrix. Taking into account this guideline, a final composite was prepared by filling a PDMS matrix with aligned Fe nanofibers in order to assess the interest of such composites for microfluidic devices.

2. Materials and methods

2.1 Magnetic filaments

All solutions of this study contained at least an iron salt, iron(III) nitrate nonahydrate (98% of purity, Sigma Aldrich), or iron(II) acetate (Sigma Aldrich), and an electrospinnable polymer which can be polyvinyl pyrrolidone (PVP, Mw ~ 1 300 000 Da, Acros Organics) or polyvinyl alcohol (PVA, Mw ~ 72 000 Da, Chang Chun Petrochemical Co.) (**Table S1**).

Fe solutions: The solution with iron salt solely contained 9 wt% of PVA in deionised water and 0.768 g of iron nitrate ($m_{PVA}/m_{iron}=1.5$). 4.8 mL of acetic acid (a.a.) was then added to 5mL of the previous solution.

Fe-Co solution: in 7 mL of absolute ethanol, PVP was first dissolved (10 wt%) before adding 0.283 g of iron acetate and 0.236 g of cobalt nitrate (Sigma Aldrich) ($n_{Fe}/n_{Co}=2$). Then, 1.5 mL of a.a. and 0.7 mL of deionized water were finally added to the previous mixture.

Fe-Ni solution: 0.329 g of iron acetate was dissolved in 7 mL of a solution containing 7 wt% of PVP in absolute ethanol. Simultaneously, 0.275 g of nickel nitrate hexahydrate (Sigma Aldrich) was mixed with 0.5 mL of deionized water before blending the two solutions together. Finally, 1 mL of a.a. was poured to the solution.

All solutions were stirred overnight at room temperature before electrospinning experiments.

Electrospinning: After overnight stirring, transparent and homogeneous solutions containing metal salts and polymers were ready to be electrospun. The electrospinning setup was mainly composed of a syringe-pump to adjust the solution feeding rate (0.02-1 mL/h), a high voltage supplier (0-30 kV), and an aluminum foil as a sample collector (ground electrode) positioned at a few centimeters from the spinneret. The solution was loaded into a plastic syringe and then extruded through a stainless steel needle (inner diameter of 0.51 mm) connected to the high voltage supply. Filaments were produced during several hours in the air before being removed from the target and cut in different pieces hanged on a silica gibbet fixed onto a crucible, specially designed to improve the treatment's reproducibility.

Thermal treatment: Heat treatments in the air were performed in a muffle furnace. Regarding Fe-based filaments, those made with PVP were pyrolysed 4h at 550°C (5°C/min) whereas those containing PVA were treated during 5h at 500°C (2°C/min). For samples containing Fe and Co or Ni, a higher temperature of treatment was set: 2h at 800°C for Fe-Ni samples and 4h at 800°C for Fe-Co filaments, with a heating ramp of 3 °C.min^{-1} in both cases. Treatments with reducing atmosphere were carried out with a mixture of argon and hydrogen (Ar/H$_2$, 90/10 or 95/5) in a tubular furnace (3°C.min^{-1}, 400°C, 1h), with a gas flow rate ranging from 0.4 to 0.7 L/min.

2.2 Composites with PDMS matrix

The best nanofiber candidate was used as filler to realize magnetic composite. The dispersion of synthesised nanofibers (0.23 wt%) into PDMS prepolymer (Sylgard from Samaro) was performed using an ultrasonic processor (Sonics Materials^{TM}, 500W, tapered 3 mm diameter sonotrode). Sonication conditions were the following: 25% amplitude, 30 seconds cycles with a 33% duty cycle for 10 min. The bucket containing the mixture was positioned in a beaker filled with ice in order to limit the rise in temperature due to sonication. Then, the curing agent was thoroughly mixed with the mixture, with a ratio 10/1 w/w of monomer/curing agent. The composite membranes of circular and square shapes, 5 mm diameter and diagonal respectively, were obtained using molds realized with dry 50 µm thick photoresist (Ethertec ®). We poured the composite on the mold and removed the excess with a blade. The reticulation was performed in an oven at 70 °C for 3 hours. During reticulation, the first batch of composite membranes was submitted to a 130 mT uniform magnetic field, created in the gap of two permanent magnets, in order to align nanofibers. The second

batch of the composite membranes was reticulated without the presence of a magnetic field.

2.3 Characterization techniques

The morphology of the electrospun filaments was characterized by scanning electron microscopy SEM (FEI, Quanta FEG 250) and by transmission electron microscopy TEM (JEOL, 2100F). For SEM observations, samples were fixed on aluminum holders covered with carbon tape before deposition of a gold-palladium coating (5 nm) by sputtering. For TEM samples, a small amount of fibers is dispersed in ethanol, and using the same ultrasound probe as the one above-mentioned for the composite preparation. Two drops of this solution are consecutively deposited onto a TEM grid (copper grid with a carbon membrane) before observation. Additional crystalline information was brought by X-ray diffraction (XRD) experiments (Philipps PW 3040/60 PANalytical X'Pert PRO (CuKα radiation; λ = 1.5406 Å at 40 kV and 30 mA). The average crystallite size was calculated with the Scherrer method. Moreover, the magnetic properties were investigated with a Quantum Design SQUID magnetometer to obtain the magnetization hysteresis loops at 310 K in a magnetic field of 40 kOe. For magnetization measurements, fibers were directly poured into a capsule, whereas composite films were placed on a silicon substrate.

Confocal observations were performed on composites, with a confocal microscope (Zeiss LSM 800), placing a composite slice between two glass slides. For 3D reconstruction, a series of 9 images were acquired, with a distance of 6 µm along the z axis between each image. Each image was an average of 2 images using the software (ZEN) function "averaging". Finer observations of composites were carried out using a

FIB/SEM workstation (NVision 40; Carl Zeiss Microscopy GmbH, Oberkochen, Germany) combining a SIINT zeta FIB column (Seiko Instruments Inc. NanoTechnology, Japan) with a Gemini I SEM column. The NVision 40 platform is also equipped with a multi-nozzle SIINT gas injection system. The angle between the FIB and SEM columns was 54°. FIB/SEM nano-tomography (FIB-nt) was performed following a precise protocol (see Supporting Information).

3. Results and discussion

3.1 Microstructural properties

Each material was prepared after the optimization of its electrospinning and thermal treatment parameters. Detailed conditions are presented in Table S1 (see Supporting Information). According to the kind of gas flowing into the furnace, iron, nickel and cobalt salts were either oxidized (under air) or reduced (under Ar/H$_2$). Thermal treatment in air at 550°C of electrospun filaments made of PVA and iron nitrate leads to the crystallization of pure α-Fe$_2$O$_3$ (hematite) (**Fig. 1**). A fine analysis of the pattern excluded any presence of γ-Fe$_2$O$_3$ (maghemite). A subsequent treatment under reducing atmosphere (Ar/H$_2$) allowed to deoxidize the material into Fe$_3$O$_4$, and even in pure iron (ferrite) when the amount of hydrogen was raised from 5 to 10%.

For filaments prepared with an iron amount twice that of Co or Ni, the resulting material had the same Fe/Ni ratio, leading to CoFe$_2$O$_4$ and NiFe$_2$O$_4$ phases, respectively. By deoxidizing NiFe$_2$O$_4$ at 600°C under Ar/H$_2$ (95/5), another material was achieved (see **Fig. S1** and **Fig. S2**). Three peaks on the XRD pattern of the corresponding sample, named "FeNi", were present. The peaks at 2 theta values of 43.6° and 50.8° correspond to the phase Fe$_{0.64}$Ni$_{0.36}$ (JCPDS sheet: 00-047-1405), with a

perfect difference of relative intensity between the two peaks, as reported in the JCPDS sheet. The peak at 44.6° can be assigned to the presence of $Fe_{0.94}Ni_{0.06}$ (Kamacite, JCPDS sheet: 00-037-0474) and/or to pure Fe (Ferrite, JCPDS sheet: 00-006-0696). Moreover, taking first into account the relative intensities, we can assume that the amount of the $Fe_{0.64}Ni_{0.36}$ phase is in the majority. Then, since the pristine n_{Fe}/n_{Ni} ratio of the material equaled 2, we can guess that an excess of iron should denote the presence of pure iron, explaining the peak present at 44.6°. Considering the Fe-Co-based alloy, the peak located at 44.7° was assigned to the presence of metallic cobalt-iron alloy (Co_3Fe_7) (**Table S3**). This compound could be assigned to a local lack of oxygen during the thermal treatment because of the presence of PVP chains, which are made of a large amount of carbon. In turn, Co_3Fe_7 is an appealing material as it is expected to exhibit a higher magnetization than pure Fe. According to the Slater-Pauling curve that describes the average atomic magnetic moments in binary alloys of the 3d transition metal series, against the number of valence (3d+4s) electrons, Co_3Fe_7 would lead to a magnetization in the excess of 1900 kA/m[31]. However, our attempts to form metallic structures by annealing of the $CoFe_2O_4$ filaments under a reducing atmosphere did not fully eliminate the oxide phase, which led to mixed structures with a relatively low magnetization. In the following only single phase structures will be discussed.
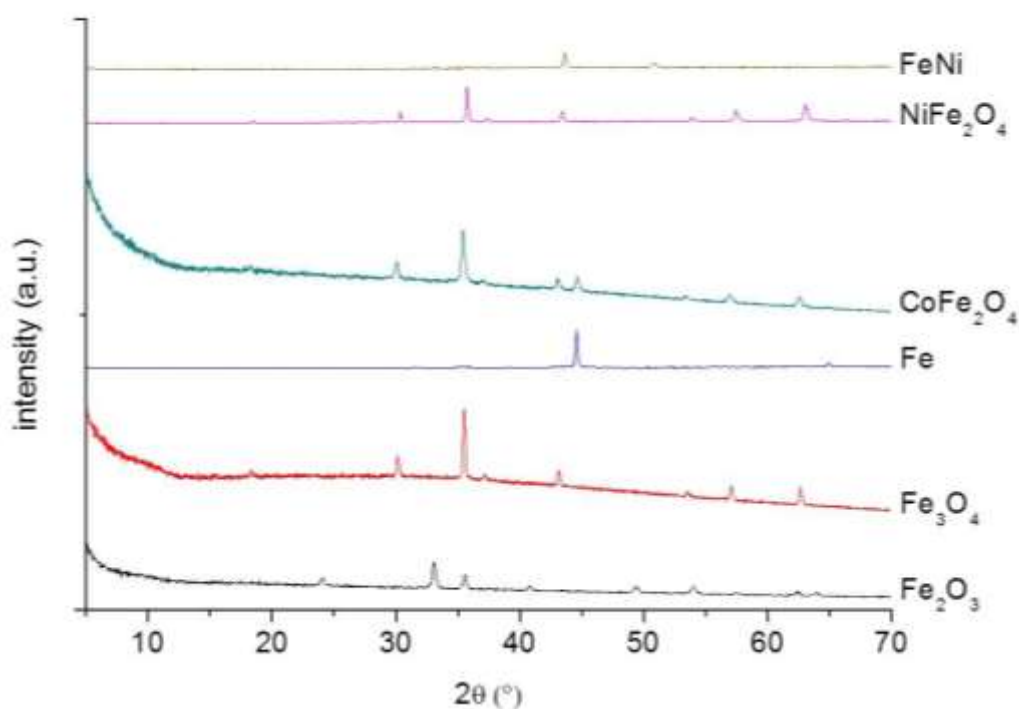
Figure 1: XRD spectra of samples after heat treatment; α-Fe₂O₃ (Rhombohedral, space group: R-3c): treatment of filaments containing PVA and iron nitrate under air, 5h at 550°C; Fe₃O₄ (Cubic, space group: Fd-3m): treatment of Fe₂O₃ sample at 400°C (1h) under Ar/H₂ (95/5); Fe (Cubic, space group: Im-3m): treatment of Fe₂O₃ sample at 400°C (1h) under Ar/H₂ (90/10); CoFe₂O₄ (Cubic, space group: Fd-3m): treatment of filaments containing PVP, iron acetate and cobalt nitrate under air, 4h at 800°C; NiFe₂O₄ (Cubic, space group: Fd-3m): treatment of filaments containing PVP, iron acetate and nickel nitrate under air, 2h at 550°C; FeNi (Cubic, space group: Fm-3m): treatment of NiFe₂O₄ sample at 600°C (1h) under Ar/H₂ (95/5).

The average crystallite size was calculated from the XRD patterns with the Scherrer method (Table S2). The crystals of all samples are assumed to have a spherical shape (due to the calculation method), with a diameter ranging from 30 to 70 nm. These values are in good agreement with our observations in a transmission electron microscope. On SEM pictures (**Fig. 2**), elongated structures were observed with a

diameter lower than 500 nm, except for the FeNi sample that did not present any fibrous morphology after treatment under Ar/H$_2$ (90/10) of NiFe$_2$O$_4$ filaments. It is noteworthy that fibers of Fe$_2$O$_3$, Fe$_3$O$_4$ and pure Fe have a diameter which is lower than 100 nm. Thus, these three materials can be named as "nanofibers". Some particles of the Fe sample have a rounded shape. In this specific case, the reducing atmosphere induces a loss of oxygen that can lead to a particle coalescence explaining the decrease of the aspect ratio of the fibers.
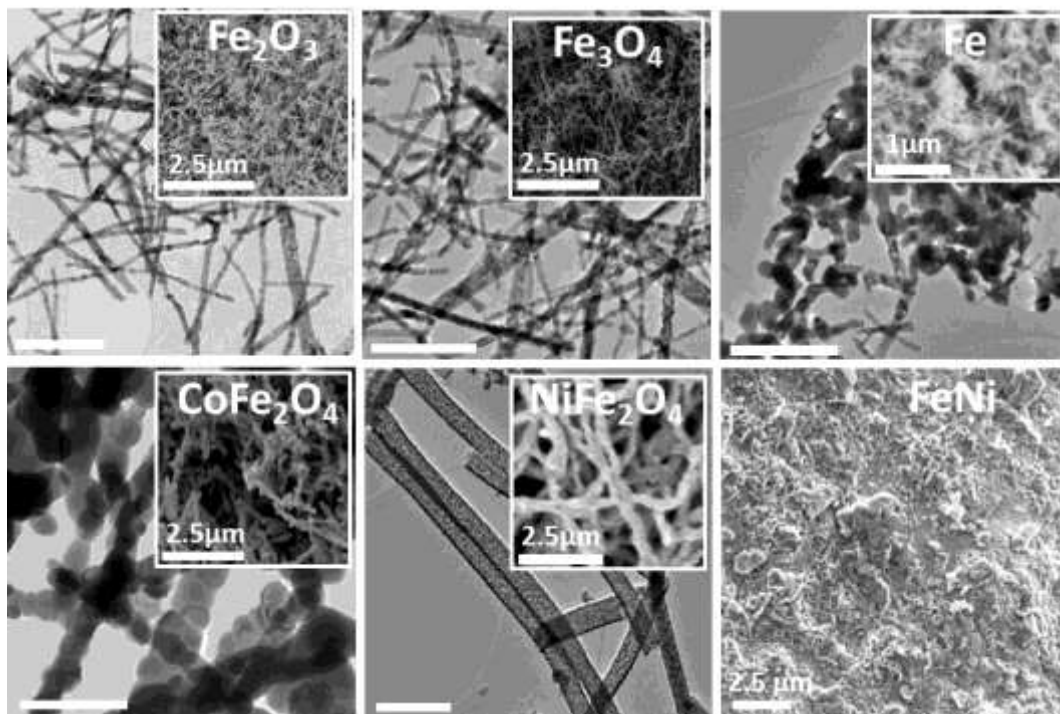
Figure 2: *TEM pictures of electrospun samples after thermal treatment; Insets correspond to SEM pictures of the corresponding samples; Scale bars of TEM pictures: 500 nm.*

3.2 Magnetic properties

We investigated the influence of the shape and microstructure of the synthesized nanofibers on their magnetic properties, in a SQUID magnetometer. We measured room temperature magnetization curves *M-H* of nanofibers.

In **table 1**, we present the magnetization of the different fibers and compare with bulk values. The spontaneous magnetization for each compound is comparable with bulk values showing that the metallic phases are relatively pure, and that potential oxidation remains limited. In particular, the largest discrepancy is measured for Fe fibers, in which the magnetization is 21% less than the one of bulk Fe. As compared to previous work on Fe nanofibers the magnetization of our fibers is relatively large [22]. Considering a fiber diameter of 48 nm that is the crystallite size determined by XRD, the magnetization reduction would correspond to a superficial "magnetically dead" layer of less than 3 nm thick.

Fe_2O_3 fibers exhibit extremely small net magnetization, confirming the predominant antiferromagnetic α-Fe_2O_3 (hematite) phase with respect to ferromagnetic γ-Fe_2O_3 (maghemite) phase as observed on the XRD pattern.

Table 1: _Fiber spontaneous magnetizations at room temperature. Comparison with bulk values._

Material	σ_s exp. (emu/g)	σ_s bulk (emu/g)
Fe	171	218[32]
NiFe	143	146.7[33]*
$\alpha-Fe_2O_3$	<2.5	0.5 [31]
Fe_3O_4	94	92[23]
$CoFe_2O_4$	84.5	80 [23]
$NiFe_2O_4$	88.6	50 [23], 55 [34]

* estimated from ref.[35]

Metallic and oxide fibers show drastically different magnetic behaviors, as reveal the _M-H_ loops of **figure 3**. Oxide fibers exhibit magnetization hysteresis while metallic Fe, Fe-Ni fibers show nearly reversible magnetization reversal process, as could be

expected considering the intrinsic magnetic properties of these materials. Indeed, coercivity highly depends on the material's microstructure and its intrinsic magnetic hardness. The magnetic hardness is characterized by a dimensionless parameter that is the ratio of anisotropy to dipole energy and scales with $\sqrt{|K_1|}/M_S$ [26]. **Table 2** shows that the oxide compounds present larger magnetic hardness values as compared to Fe and FeNi favoring the larger coercive field. One can notice that the coercive field can be under-estimated since the nanofibers are not rigidly fixed into the capsule during SQUID measurement.
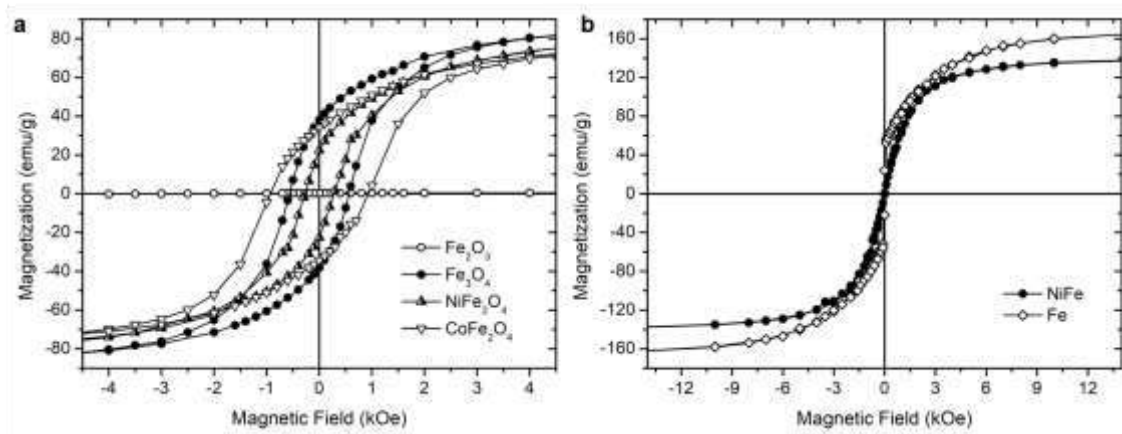
Figure 3: *Room temperature magnetization curves of fibers: (a) Fe$_3$O$_4$, Fe$_2$O$_3$, CoFe$_2$O$_4$, NiFe$_2$O$_4$, (b) Fe, NiFe.*

Besides microstructure considerations would favor larger coercivity in oxide fibers. Based on XRD Debye Scherrer analysis (**Table S2**), the crystallites size ranges from 30 to 70 nm independently to the material. This is in the critical range of the magnetic domain length scale. The general picture that describes the dependence of coercive field with particle size presents a maximum at the critical size that separates single domain to multidomain structure.[36][31] The crystallites size is comparable to the maximum single domain particle size of oxides, if not smaller, but greater than the one of the considered metals. As a result, one could expect the magnetic structure to break

into multidomain structure in metallic fibers but to remain single domain in oxides, which again favors coercivity.

Both Fe and NiFe fibers show no hysteresis but exhibit different *M-H* loop shapes. The magnetization reversal of NiFe fibers is progressive while the it occurs in a two-step process for Fe fibers, with an abrupt magnetization change in the low field region followed by a progressive approach to saturation.

__Table 2__: Magnetic properties and grain size of synthesized fibers. Comparison with intrinsic magnetic properties of the materials.

Materials	Coercive field (kOe)	Magnetic hardness parameter	XRD crystallite size (nm)	Maximum single domain particle size (nm) [37]
Fe		0.12	48	10
NiFe		0.1	40	1.6
Fe_3O_4	0.57	0.84	47	38
$CoFe_2O_4$	0.93	0.21	30	160
$NiFe_2O_4$	0.28	0.48*	67	-

* calculated assuming same density between $CoFe_2O_4$ and $NiFe_2O_4$

In both cases, the saturation of the magnetization is reached for an applied field of around 10 kOe. This is significantly larger than the expected anisotropy field from the intrinsic magnetocrystalline contribution (inferior to 1 kOe in Fe and less in Fe-Ni alloys). This shows that the predominant contribution to the anisotropy is not of magnetocrystalline origin, but could be the contribution of the fiber shape and the microstructure.

In addition, provided the lower magnetization of Fe fibers as compared to bulk Fe, one cannot discard a secondary phase, like Fe-O formed at the fibers' surface.

3.3 Magnetic composite polymer

Fe nanofibers/PDMS composite were realized with a concentration of 0.23 wt%. When no magnetic field was applied during the polymer reticulation, nanofibers were distributed in disorder in the polymer matrix. However, when an external magnetic field was applied, nanofibers have self-ordered in chain-like agglomerates. The magnetic pattern and the exposure time of the composite to this pattern influence the organization of the fibers [38]. These first experiments subjected the composite to a homogeneous magnetic field of 130 mT and a time of 2 hours, corresponding to the cross-linking time of the PDMS matrix.

Before complete PDMS reticulation, nanofibers orient themselves relatively to the magnetic field, and dipolar interactions guide the fibers motion: (i) dipole-dipole attraction in the direction of the applied field forming high aspect ratio chains along the flux lines and (ii) dipole-dipole repulsion within the orthogonal plane to the applied field vector leading to a self-distancing between adjacent chains[39]. We studied nanofiber organization using confocal microscopy and FIB/SEM (**see part 4 of S.I.**). These complementary experiments enable to perform 3D structural characterization of the composite at different scales. Confocal microscopy allows observing a composite volume of 620 x 620 x 50 µm³ with a voxel of 500 x 200 x 200 nm³ and FIB/SEM a composite volume of 23.25 x 17.52 x 15.7 µm³ with a voxel of 25x25x25 nm³. Confocal microscopy gives an overview of the nanofiber composite organization in the polymer matrix. **Fig. 4-a** shows Fe nanofibers self-ordered in elongated chains in the PDMS matrix. Chain diameters range from µm to tens of µm, they are aligned along the magnetic flux lines. The distribution of the chains in the volume is rather

homogeneous as chains are present over the entire thickness and surface of the sample, as shown in **Fig. 4-b**. FIB/SEM allows to have a closer look at the morphology and orientation of the agglomerates (**Fig. 4-c**). Visible chain-like agglomerates possess a high aspect ratio with a diameter of the order of 2 µm, and are localized at different thicknesses of the composite, as highlighted by Confocal microscopy. Although both chains are oriented in the same direction, we can observe a slight angular dispersion, which could be due to the repulsive force of the neighboring chains, on top of the image.
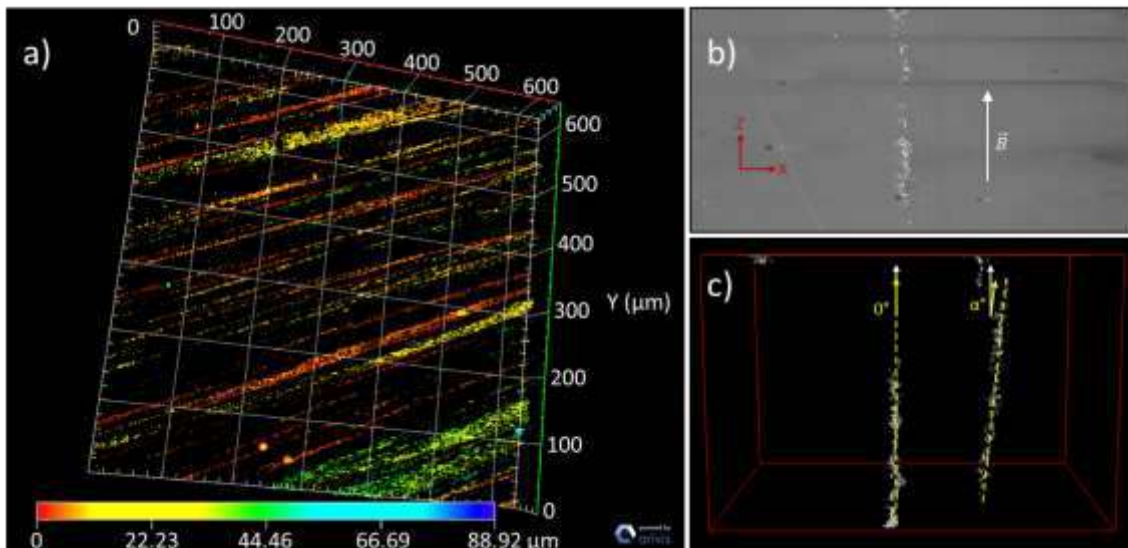
Figure 4: a) 3D reconstruction of confocal images of the composite (PDMS + Fe fibers), the thickness of the sample being of about 50 µm; b) is a reconstructed image in the XZ plane from the SEM images acquired between each FIB slicing (top view), B vector indicating the direction along which the external magnetic field was applied during the composite fabrication; c) 3D reconstruction of FIB images of the composite, with dashed lines along the chain axis and values of the corresponding angles between those lines and the B vector.

The fibers' alignment leads to an anisotropic response, as shown in **Fig. 5**. As expected from magnetostatic energy considerations, the easy magnetization axis is found along the global orientation of the nanofibers. However, as compared to other work on oriented Fe and Co nanofibers [40] the anisotropy is less pronounced. The relatively low reduced remanence along the easy axis, below 50%σ_s, and weaker anisotropic response could be explained by the presence of superparamagnetic domains. Indeed the nanocrystals in the present work are smaller, so the population of superparamagnetic grains is expected to be larger.
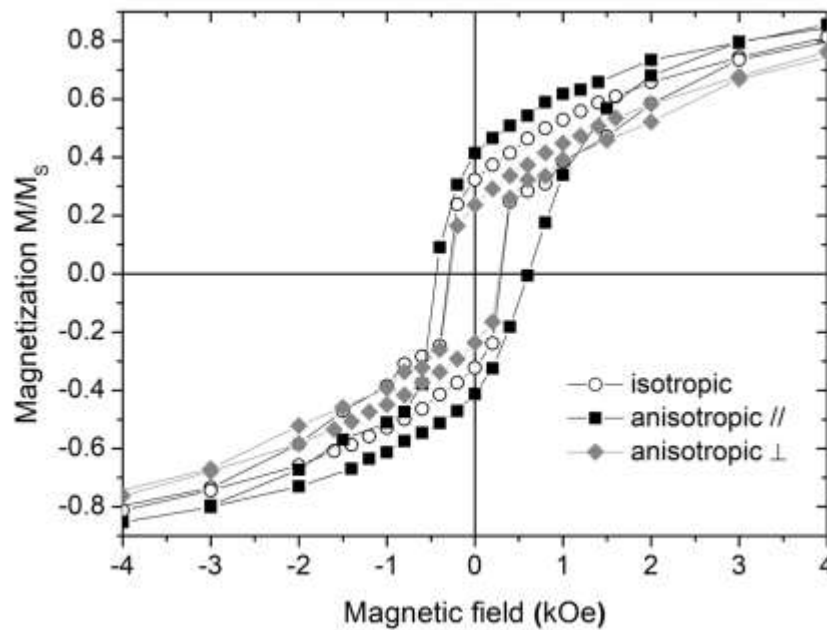
Figure 5: Magnetization of composites with isotropic fibers orientation (white circle), and with aligned fibers, measured along the fiber (black square) and perpendicular to the fiber (grey diamond).

Taking into account the shape of the pure iron fibers (**Fig. 2**), during the thermal treatment, fibers with elongated shapes can merge and form 3D multi-branched structures. Thus, the initial expected uniaxial shape anisotropy of individual fibers can

be biased. In these 3D structures, the easy-magnetization direction is expected to be the best compromise between all the contributions of the constituting branches.

4. Conclusions

Fibers of different magnetic materials, metals, Fe and FeNi, and oxides Fe_3O_4, Fe_2O_3, $CoFe_2O_4$, $NiFe_2O_4$, were produced using electrospinning. Their morphology was characterized by SEM and TEM and additional crystalline information were obtained by X-ray diffraction (XRD) experiments. Except for FeNi sample that did not present any fibrous morphology after heating treatment, Fe, Fe_3O_4, Fe_2O_3, $CoFe_2O_4$ and $NiFe_2O_4$, fibers shown diameter lower than 500 nm. The average crystallite size, calculated from the XRD patterns with the Scherrer method, ranged from 30 to 70 nm. Concerning magnetic properties, metallic and oxide fibers presented drastically different magnetic behaviors, in agreement with the intrinsic magnetic properties of these materials.

We have thus succeeded in synthesizing pure iron nanofibers that have a magnetization at saturation of 171 emu/g, no hysteresis and a diameter lower than 100nm. These NFs are excellent candidates for the realization of magnetic composite polymers. We have performed first experiments by integrating these filaments in a PDMS matrix at a concentration of 0.23 wt%, and a magnetic field was applied during reticulation to self-organize iron fibers in the matrix. As shown by 3D structural characterization, performed by FIB-nt and confocal microscopy, Fe nanofibers self-ordered in elongated agglomerates in the PDMS matrix when a magnetic field was applied during composite cross-linking. Such alignment of the fibers leads to an enhanced anisotropic magnetic response. Such magnetic multifunctional material is promising for numerous applications.

Acknowledgments

References

[1]   J. Thévenot, H. Oliveira, O. Sandre, S. Lecommandoux, Magnetic responsive polymer composite materials, Chem. Soc. Rev. 42 (2013) 7099–7116. doi:10.1039/c3cs60058k.

[2]   F.N. Pirmoradi, J.K. Jackson, H.M. Burt, M. Chiao, A magnetically controlled MEMS device for drug delivery: Design, fabrication, and testing, Lab Chip. (2011). doi:10.1039/c1lc20438f.

[3]   M. Nikkhah, F. Edalat, S. Manoucheri, A. Khademhosseini, Engineering microscale topographies to control the cell-substrate interface, Biomaterials. 33 (2012) 5230–5246. doi:10.1016/j.biomaterials.2012.03.079.

[4]   J. Le Digabel, N. Biais, J. Fresnais, J.F. Berret, P. Hersen, B. Ladoux, Magnetic micropillars as a tool to govern substrate deformations, Lab Chip. 11 (2011) 2630–2636. doi:10.1039/c1lc20263d.

[5]   R.M. Erb, J.J. Martin, R. Soheilian, C. Pan, J.R. Barber, Actuating Soft Matter with Magnetic Torque, Adv. Funct. Mater. 26 (2016) 3859–3880. doi:10.1002/adfm.201504699.

[6]   R.M. Erb, J.S. Sander, R. Grisch, A.R. Studart, Self-shaping composites with programmable bioinspired microstructures, Nat. Commun. 4 (2013) 1–8. doi:10.1038/ncomms2666.

[7]   A. Alfadhel, B. Li, A. Zaher, O. Yassine, J. Kosel, A magnetic nanocomposite for biomimetic flow sensing, Lab Chip. 14 (2014) 4362–4369. doi:10.1039/c4lc00821a.

[8]   M. Faivre, R. Gelszinnis, J. Degouttes, N. Terrier, C. Rivière, R. Ferrigno, A.-L. Deman, Magnetophoretic manipulation in microsystem using carbonyl iron-

polydimethylsiloxane microstructures, Biomicrofluidics. 8 (2014) 054103. doi:10.1063/1.4894497.

[9]   X. Yu, C.Y. Wen, Z.L. Zhang, D.W. Pang, Control of magnetic field distribution by using nickel powder@PDMS pillars in microchannels, RSC Adv. 4 (2014) 17660–17666. doi:10.1039/c3ra47902a.

[10]   J. Li, M. Zhang, L. Wang, W. Li, P. Sheng, W. Wen, Design and fabrication of microfluidic mixer from carbonyl iron-PDMS composite membrane, Microfluid. Nanofluidics. 10 (2011) 919–925. doi:10.1007/s10404-010-0712-2.

[11]   J. Kim, K.N. Kang, Y. Jin, J. Goettert, P.K. Ajmera, Hydrodynamic focusing micropump module with PDMS/nickel-particle composite diaphragms for microfluidic systems, Microsyst. Technol. (2014). doi:10.1007/s00542-014-2089-8.

[12]   D. Fragouli, R. Buonsanti, G. Bertoni, C. Sangregorio, C. Innocenti, A. Falqui, D. Gatteschi, P.D. Cozzoli, A. Athanassiou, R. Cingolani, Dynamical formation of spatially localized arrays of aligned nanowires in plastic films with magnetic anisotropy, ACS Nano. (2010). doi:10.1021/nn901597a.

[13]   A. Tokarev, J. Yatvin, O. Trotsenko, J. Locklin, S. Minko, Nanostructured Soft Matter with Magnetic Nanoparticles, Adv. Funct. Mater. 26 (2016) 3761–3782. doi:10.1002/adfm.201504443.

[14]   S. Ghosh, I.K. Puri, Soft polymer magnetic nanocomposites: Microstructure patterning by magnetophoretic transport and self-assembly, Soft Matter. 9 (2013) 2024–2029. doi:10.1039/c2sm27420e.

[15]   S. Marchi, A. Casu, F. Bertora, A. Athanassiou, D. Fragouli, Highly Magneto-Responsive Elastomeric Films Created by a Two-Step Fabrication Process, ACS

Appl. Mater. Interfaces. 7 (2015) 19112–19118. doi:10.1021/acsami.5b04711.

[16]   A.L.D.S. Mekkaoui, D.D.J.F. Chateaux, Anisotropic composite polymer for high

magnetic force in microfluidic systems, Microfluid. Nanofluidics. (2017) 1–7.

doi:10.1007/s10404-017-2008-2.

[17]   S. Mekkaoui, D. Le Roy, M.C. Audry, J. Lachambre, V. Dupuis, J. Desgouttes, A.L.

Deman, Arrays of high aspect ratio magnetic microstructures for large trapping

throughput in lab-on-chip systems, Microfluid. Nanofluidics. (2018).

doi:10.1007/s10404-018-2141-6.

[18]   S. Hosic, S.K. Murthy, A.N. Koppes, Microfluidic Sample Preparation for Single

Cell Analysis, Anal. Chem. 88 (2016) 354–380.

doi:10.1021/acs.analchem.5b04077.

[19]   V. Narayanamurthy, S. Nagarajan, A.Y. Firus Khan, F. Samsuri, T.M. Sridhar,

Microfluidic hydrodynamic trapping for single cell analysis: Mechanisms,

methods and applications, Anal. Methods. 9 (2017) 3751–3772.

doi:10.1039/c7ay00656j.

[20]   D. Le Roy, D. Dhungana, L. Ourry, M. Faivre, R. Ferrigno, A. Tamion, V. Dupuis, V.

Salles, A.L. Deman, Anisotropic ferromagnetic polymer: A first step for their

implementation in microfluidic systems, AIP Adv. 6 (2016).

doi:10.1063/1.4943927.

[21]   K. Keshoju, L. Sun, Mechanical characterization of magnetic nanowire-

polydimethylsiloxane composites, J. Appl. Phys. (2009). doi:10.1063/1.3068173.

[22]   V. Vega, T. Böhnert, S. Martens, M. Waleczek, J.M. Montero-Moreno, D. Görlitz,

V.M. Prida, K. Nielsch, Tuning the magnetic anisotropy of Co–Ni nanowires:

comparison between single nanowires and nanowire arrays in hard-anodic

aluminum oxide membranes, Nanotechnology. 23 (2012) 465709. doi:10.1088/0957-4484/23/46/465709.

[23] R.B. Rakhi, W. Chen, D. Cha, H.N. Alshareef, Substrate dependent self-organization of mesoporous cobalt oxide nanowires with remarkable pseudocapacitance, Nano Lett. (2012). doi:10.1021/nl300779a.

[24] H. Kyoung, K.Æ. Hak, Y. Kim, Production of beads like hollow nickel oxide nanoparticles using colloidal-gel electrospinning methodology, (2008) 860–864. doi:10.1007/s10853-007-2190-9.

[25] C. Eid, A. Brioude, V. Salles, J.-C. Plenet, R. Asmar, Y. Monteil, R. Khoury, A. Khoury, P. Miele, Iron-based 1D nanostructures by electrospinning process, Nanotechnology. 21 (2010) 125701. doi:10.1088/0957-4484/21/12/125701.

[26] C. Eid, D. Luneau, V. Salles, R. Asmar, Y. Monteil, A. Khoury, A. Brioude, Magnetic properties of hematite nanotubes elaborated by electrospinning process, J. Phys. Chem. C. (2011). doi:10.1021/jp203426j.

[27] Y. Ju, J. Park, H. Jung, S. Cho, W. Lee, Fabrication and characterization of cobalt ferrite (CoFe 2 O 4) nanofibers by electrospinning, 147 (2008) 7–12. doi:10.1016/j.mseb.2007.10.018.

[28] D. Li, T. Herricks, Y. Xia, Magnetic nanofibers of nickel ferrite prepared by electrospinning, 4586 (2013) 10–13. doi:10.1063/1.1630844.

[29] T. Fiorido, J. Galineau, V. Salles, L. Seveyrat, F. Belhora, P.J. Cottinet, L. Hu, Y. Liu, B. Guiffard, A.B. Van De Moortele, T. Epicier, D. Guyomar, A. Brioude, Bifunctional organic/inorganic nanocomposites for energy harvesting, actuation and magnetic sensing applications, Sensors Actuators, A Phys. (2014). doi:10.1016/j.sna.2014.02.010.

[30]   H. Shao, X. Zhang, S. Liu, F. Chen, J. Xu, Y. Feng, Preparation of pure iron
        nanofibers via electrospinning, Mater. Lett. 65 (2011) 1775–1777.
        doi:10.1016/j.matlet.2011.03.049.

[31]   J.M.D. Coey, Micromagnetism, domains and hysteresis, in: Magn. Magn. Mater.,
        Cambridge University Press, 2001: pp. 231–263.
        doi:10.1017/CBO9780511845000.008.

[32]   F.-D. Delapierre, G. Mottet, V. Taniga, J. Boisselier, J. Viovy, L. Malaquin, F.
        Delapierre, G. Mottet, V. Taniga, J. Boisselier, J. Viovy, L. Malaquin, High
        throughput micropatterning of interspersed cell arrays using capillary assembly,
        Biofabrication. 9 (2017) 015015. doi:10.1088/1758-5090/aa5852.

[33]   N. Islam, M. Abbas, C. Kim, Synthesis of monodisperse and high moment nickel
        iron (NiFe) nanoparticles using modified polyol process, Curr. Appl. Phys. 13
        (2013) 2010–2013. doi:10.1016/j.cap.2013.08.020.

[34]   C.N. Chinnasamy, A. Narayanasamy, N. Ponpandian, Mixed spinel structure in
        nanocrystalline NiFe2O4, 63 (2001) 2–7. doi:10.1103/PhysRevB.63.184108.

[35]   J.M.D. Coey, Advances in Magnetics Hard Magnetic Materials : A Perspective, 47
        (2011) 4671–4681.

[36]   X. Xu, Z. Li, N. Kotagiri, P. Sarder, S. Achilefu, A. Nehorai, Microfluidic
        microsphere-trap arrays for simultaneous detection of multiple targets, in:
        Microfluid. BioMEMS, Med. Microsystems XI, 2013. doi:10.1117/12.2006628.

[37]   J. Nilsson, M. Evander, B. Hammarström, T. Laurell, Review of cell and particle
        trapping in microfluidic systems, Anal. Chim. Acta. 649 (2009) 141–157.
        doi:10.1016/j.aca.2009.07.017.

[38]   L. Zhu, D. Xie, J. Ma, J. Shao, X. Shen, Fabrication of polydimethylsiloxane

composites with nickel particles and nickel fibers and study of their magnetic

properties, Smart Mater. Struct. 22 (2013). doi:10.1088/0964-

1726/22/4/045015.

[39]   S. Odenbach, Ferrofluids: magnetically controllable fluids and their applications,

2008.

[40]   M. Graeser, M. Bognitzki, W. Massa, C. Pietzonka, A. Greiner, J.H. Wendorff,

Magnetically anisotropic cobalt and iron nanofibers via electrospinning, Adv.

Mater. 19 (2007) 4244–4247. doi:10.1002/adma.200700849.